A one dimensional model for Hollow Cathode Orifice life time prediction

IEPC-2019

Franco Bosi [1], Francesco Guarducci [2] and Stephen B. Gabriel[3]

Mars Space Ltd, Southampton, SO145FF, United Kingdom

Lifetime assessment of Hollow Cathode (HC) sources is a resource demanding process, both experimentally, due to the large amount of hours space qualification requires, and numerically due to the complexity and high computational times associated to 2D plasma fluid codes available in literature. We present a 1D orifice - 0D insert model developed for lifetime prediction of the HC in terms of orifice erosion; the resulting lower computational costs makes the code fast for design and optimization studies of HC geometries. Beginning of life simulations are compared against the numerical data presented in [6]; a modified sputtering yield curve is derived, similar to the one proposed in [9] and the role of anomalous resistivity is briefly discussed. The time evolution of the orifice channel confirm the expected asymptotic decrease of the erosion rate.

Nomenclature

A	=	Cross sectional area	R	=	Orifice Radius
a	=	Anomalous resistivity coefficient	R_g	=	Gas constant
D_a	=	Ambipolar diffusion coefficient	S_e	=	Ionization energy losses
D_0	=	Neutral diffusion coefficient	S_{iz}	=	Ionization charge production
E	=	Electric field	T	=	Gas temperature
e	=	Electron charge	T_e	=	Electron temperature
$H(T_w)$	=	Emitter thermal power loss function	U_i	=	Ionization energy
I_d	=	Insert net current	u_0	=	Neutral flow velocity
I_e	=	Electron current	u_b	=	Ion Bohm velocity
I_{em}	=	Electron emitter current	u_r	=	Ion radial velocity
I_{ew}	=	Electron wall loss current	v_{eth}	=	Electron thermal velocity
I_i	=	Ionic current	ρ	=	Neutral density
I_{iz}	=	Ionization current (charge generation rate)	φ	=	Plasma potential
I_w	=	Wall current	φ_s	=	Insert sheath potential
k_e	=	Electron thermal conductivity	φ_w	=	Emitter work function
k_{ne}	=	Electron Knudsen number	η	=	Plasma resistivity
M	=	Xe atomic mass	λ_{01}	=	First zero of first kind Bessel function
n	=	Plasma density	ν_{ei}	=	Electron-ion collision frequency
p	=	Neutral pressure	ν_{iz}	=	Ionization collision frequency
p_e	=	Electron pressure	μ	=	Dynamic viscosity
P_{ew}	=	Electron wall energy loss	μ_e	=	Electron mobility
Q_t	=	Thermal energy exchange source term	μ_i	=	Ion mobility
Q_r	=	Friction energy exchange source term	ω_{pe}	=	Electron plasma frequency

[1] Research Engineer, franco.bosi@mars-space.co.uk
[2] Senior Research Engineer, francesco.guarducci@mars-space.co.uk
[3] Director, stephen.gabriel@mars-space.co.uk

I. Introduction

The Hollow Cathode (HC) is an electron source device widely adopted in Electric propulsion systems for satellites, such as Gridded Ion Engines and Hall Effect Thrusters[1]. This device can be used main electron source responsible for the plasma formation inside the thruster chamber, or as beam neutralizer for the positive flux of ions ejected by the propulsion system. HC are critical components as they need to be able to operate for thousands of hours; depending on the geometrical dimensions and the current density achieve by the HC the orifice channel can be subject to substantial erosion caused by ion sputtering of the refractory metal wall.

NSTAR Neutralizer (NHC) orifice erosion was observed during the life time test performed by NASA between 1997 and 2004 [2]; after 8200 h of operation the observed erosion consisted to almost twice the original diameter of the channel. The same life time test experiment shown that the main discharge cathode (DHC) was not affected by orifice wall erosion, it was, however, affected by considerable erosion on the external keeper surface.

HC for EP applications have been subject to considerable investigation, both from experimental and modelling point of view. Global models (0D) are available in literature [3,4] both for parameter operation prediction and study optimization, a critical review on 0D modelling for HC is presented in [5]. One dimensional hollow cathode models are presented in [6,7,8]; the model presented by Katz[6] in 2003 is constituted by a 0D description of the insert region coupled to a 1D –fluid description of the orifice region and represent the base-ground of the work presented here, in that paper the author address qualitatively the phenomena of the erosion on the NSTAR NHC.

Mikellides et al. [9] and Sari et al. [10] developed a fully two-dimensional numerical model able to describe the whole HC system, for physical investigation purposes; the authors discuss sheath conditions to apply to the emitting surface and address of anomalous resistivity caused by stream instabilities. Both models are critically evaluated against experimental plasma profiles measurements performed on the NSTAR and NEXIS HC presented in [11]. Another two dimensional HC code developed on COMSOL is presented by Liu et al. [12], the code is applied to a LaB6 HC of the STP-100 engine but no comparison with experimental data is provided.

HC 2D models are complex to develop and resource demanding; in this work we present a 1D orifice model coupled to a 0D insert model for the description of the HC, the model is flexible and low resource consuming and can be used to perform parametric studies and optimization that requires a high number of simulation runs; the model is able to predict fairly the erosion of the orifice NSTAR NHC, showing that it can be used to assess the lifetime of HC neutralizer orifices. Finally, we discuss the use of different boundary conditions for the radial diffusion of ions to the wall, namely Dirichlet and Robin boundary conditions and their effect on the plasma profiles.

II. Numerical model description

The model separate the HC in two regions: the insert and the orifice region. With reference to Figure II-1 the insert region is solved with a 0D approach and the orifice region is treated as a quasi-one dimensional problem with the cross sectional area A(x) function of the axial coordinate. The model solves the steady state continuity and energy equations in the plasma fluid approximation, with several assumptions that will be explained in each subsection.

A. Orifice plasma model

The total mass continuity equation can be expressed with respect to the sum of the neutral gas flow and the 1D axial ion current, with *M* the Xenon atomic mass and *e* the electron charge.
The total mass continuity equation can be expressed with respect to the sum of the neutral gas flow and the 1D axial ion current, with *M* the Xenon atomic mass and *e* the electron charge.

$$\nabla \cdot \left(u_0 \rho A + I_i \frac{M}{e} \right) = 0 \tag{1}$$

The Poiseuille flow approximation introduced in [6] is adopted here, it allows to express the neutral velocity in function of the pressure gradient, the radial dimension of the channel and the viscosity of the gas:

$$u_0 = -\frac{R^2}{8\,\mu}\nabla p \tag{2}$$

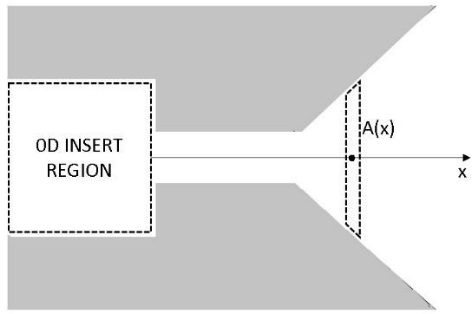

Figure II-1-Simulation domain geometry, 0D insert region and 1D orifice region.

Inserting Eq.2 in Eq.1 and neglecting the variation of gas temperature we obtain a diffusion equation for the neutrals with a diffusion coefficient defined as follow.

$$\nabla\cdot(-D_0\nabla\rho) = -\nabla\cdot\left(I_i\cdot\frac{M}{e}\right) \tag{3}$$

$$D_0 = -\frac{A^2}{8\,\mu\,\pi}\mathrm{R_g}T \tag{4}$$

The ion continuity

Quasi neutrality and drift diffusion approximation are assumed for both electrons and ions within the plasma; combining the ion and electron current expressions, as in [6], a relation for the ion current is obtained as follow:

$$I_i = (e\,n\,u_0 - eD_a\nabla n)A - \frac{\mu_i}{\mu_e}I_e \tag{5}$$

The continuity equation for the plasma density s then expressed as the divergence of the ion current, and it results in the form of a non-homogenous convection diffusion equation with S_{iz} the ionization source term and I_w the flux of positive charges that are loss at the wall :

$$\nabla\cdot(e\,n\,u_0A) + \nabla\cdot(-A\,D_a\,e\nabla n) = +S_{iz} - I_w + \nabla\cdot\left(\frac{\mu_i}{\mu_e}I_e\right) \tag{6}$$

The charge continuity

The charge continuity is used to determine the electron current I_e. In this work we adopt the convention that currents are parallel to the particle velocities, therefore $I_e = e\,n\,u_e$ and $I_i = e\,n\,u_i$. The source terms are the divergence of the 1D ion current and the flux of positive charges to the wall expressed as in Eq.7.

$$\nabla\cdot I_e = \nabla\cdot I_i + I_w \tag{7}$$

n(R) is the plasma density evaluated at the wall and u_b is the Bohm velocity; the correct expression of the current conservation (Eq.7) would contain also the flux of electrons to the wall, however, this term is negligible due to the high difference between the plasma potential and the grounded wall; we have performed simulations with the additional electron loss term, and observed that the solution remains unaffected by it.

Ion radial diffusion

The ion current impinging on the wall is calculated solving the radial diffusion equation in the ambipolar approximation. Two boundary conditions were tested in this regard:

1. Dirichlet boundary condition setting zero plasma density at the solid wall, as previously implemented in [6].
2. A Robin boundary condition representing the ions Bohm flux at the wall, as suggested in [13].

The wall current for the Dirichlet boundary case is expressed as the product of average density (along the radius) and the radial velocity evaluated at the wall [6].

$$I_w = e\, n\, u_r(R) \cdot 2\pi R \tag{8}$$

$$u_r(R) = D_a \lambda_{01}^2/(2R) \tag{9}$$

The wall current for the Robin boundary case is expressed as the product of the density evaluated at the wall) and the Bohm velocity, it requires the calculation of a γ parameter obtained solving the transcendental equation Eq.12, where $\delta = u_b R/D_a$.

$$I_w = e\, n(R) u_b \cdot 2\pi R \tag{10}$$

$$n(R) = \frac{n\, \gamma J_0(\gamma)}{2\, J_1(\gamma)} \tag{11}$$

$$-\gamma\, J_1(\gamma) + \delta J_0(\gamma) = 0 \tag{12}$$

The electron energy equation

The electron energy equations is written in the form reported by Mikellides [14]; detailed expressions for the source terms are not repeated here, the reader can find them in [14]. The term P_{ew} represent the energy losses of electrons lost at the wall, though negligible, it is important when marching the solution from the initial condition, for its stabilization effect.

$$\nabla \cdot \left(\frac{5}{2} I_e T_e - k_e \nabla T_e\right) = Q_T + Q_R + I_e \frac{\nabla p_e}{en} - P_{ew} - S_e \tag{13}$$

$$P_{ew} = \frac{1}{4}\, v_{eth} en \exp\left(-\frac{\phi}{T_e}\right) \cdot (2T_e + \phi) \cdot 2\pi R(x) \tag{14}$$

The effect of anomalous resistivity, that is implemented in 2D HC models [9,10], is included here; we adopted the expression proposed in [9], which defines an anomalous collision frequency resulting from electron-ion streaming instabilities. It affects also the electric field in the calculation of the resistivity term and the plasma potential that is derived from it.

$$\nu_a = a\, K_{ne} \omega_{pe} \tag{15}$$

$$E = -\eta\, \frac{I_e}{A} - \frac{\nabla p_e}{en} + \frac{m\nu_{ei}}{e^2 n} \cdot \frac{I_i}{A} \tag{16}$$

$$\phi(x) = \phi_{in} + \int_0^x -E \cdot dx \tag{17}$$

B. Insert plasma model

The insert region is modelled with a similar 0D approach to the one reported in [1]; it solves four equations in order to determine the insert plasma density n, the electron temperature T_e, the potential drop at the cathode sheath V_{sh} and the emitter wall temperature T_w; the gas temperature is assumed to be equal to the emitter wall temperature and the neutral density is determined by assuming Poiseuille flow in the insert and is coupled with 1D the neutral flow solution at the orifice. The solution of the 0D insert region provides inlet boundary conditions for the 1D orifice equations; the insert region equations (Eq.18-21) are the radial diffusion eigenvalue equation, the 0D energy balance, the energy balance at the emitter surface and the current balance within the insert.

$$\left(\frac{R}{\lambda_{01}}\right)^2 \cdot \nu_{iz} = D_a \tag{18}$$

$$\eta I_e^2 + \phi_s \cdot I_{em} = I_{iz} U_i + \frac{5}{2} T_e \cdot I_e + I_{ew} \cdot (2T_e + \phi_s) \tag{19}$$

$$\left(\phi_s + \frac{T_e}{2} + U_i - \phi_w\right) \cdot I_{iz} + (2T_e + \phi_w) \cdot I_{ew} = H(T_w) + I_{em} \cdot \phi_w \tag{20}$$

$$I_{iz} - I_{ew} + I_{em} = I_d \tag{21}$$

On the previous equations ν_{iz} is the ionization frequency, η the plasma resistivity, φ_s the potential sheath drop, I_{em} the emitter current, I_{ew} the electron loss to the wall, I_{iz} the ionization current, I_d is the net current entering the orifice channel, φ_w the emitter wall function and $H(T_w)$ the conduction heat loss function of the emitter.

C. Numerical integration

Boundary conditions for the 1D orifice problem are obtained from the insert 0D region and imposing the conservation of mass flow and total current on both inlet and outlet sections of the orifice. In the particular case of the charge continuity equation, solved to obtain the electron current I_e , a Newmann boundary condition is applied to the exit section and a Dirichlet boundary is applied to the inlet; the inlet value of electron current, $I_{e,in}$ is searched iteratively until the total outlet current match the nominal discharge current of the HC.
Due to the non-linearity of the equations and source terms, the model is solved with a segregated approach in which the algorithm iterates between the different module-equations until the changes in the solution field are below a designated tolerance. Explicit relaxation is applied on the solution update and implicit relaxation is applied on the system matrix of the equations, more specifically the *false transient relaxation* method reported in [16].

III. Results and discussion

The model is applied to the NSTAR NHC as it was operated on the lifetime test reported in [2]; the nominal current during the test was 3.26 A (1.5A keeper current and 1.76 beam neutralization current), the mass flow was set at 3 sccm for the first 7000 hours and then increased to 3.6 sccm for the remaining hours (7000-8200 h). The geometrical and operation parameters are summarized in Table III-1.
Beginning of life (BOL) profiles are compared with two different types of wall of boundary conditions, and a sensitivity analysis is performed on the active length parameter of the insert 0D model, and its effect on the 1D profiles of the orifice. Erosion simulations are presented in the last section, relative to the 8200 hours test reported in [2].

Table III-1- Geometrical and operation parameters for the NHC simulation

Name	Parameter	Value
Insert radius	R_c	$1.9\cdot10^{-3}$ mm
Orifice radius	R_o	$0.14\cdot10^{-3}$ mm
Orifice length (straight)	L_{str}	$0.75\cdot10^{-3}$ mm
Orifice length (chamfer)	L_{div}	$0.50\cdot10^{-3}$ mm
Orifice chamfer angle	α	45 deg
Nominal current (keeper + beam)	I_d	3.26 A
Flow rate 0-7000 h	$\dot{m}$	3 sccm
Flow rate 7000-8200 h	$\dot{m}$	3.6 sccm

A. BOL plasma profiles

Figure III-1 shows the plasma profiles obtained applying Dirichlet and Robin wall boundary conditions are almost identical; as pointed out in [13], while the Bohm flux condition is general, the Dirichlet boundary is valid in high pressures plasma. The NSTAR NHC operates at high pressures and for this reason the two solutions results superimposed. Figure II-1, also, compares the results with the profiles reported in [6]; a qualitative agreement between [6] and this work is observed. The most relevant difference is observed in the plasma density profile, with a peak density of about $3 \cdot 10^{22}$ compare to the $6 \cdot 10^{22}$ of [6]; the higher peak density of [6] results in a higher wall current $I_w \sim enu_b$, which in turns results in a lower electron current in the inlet region, due to charge conservation.

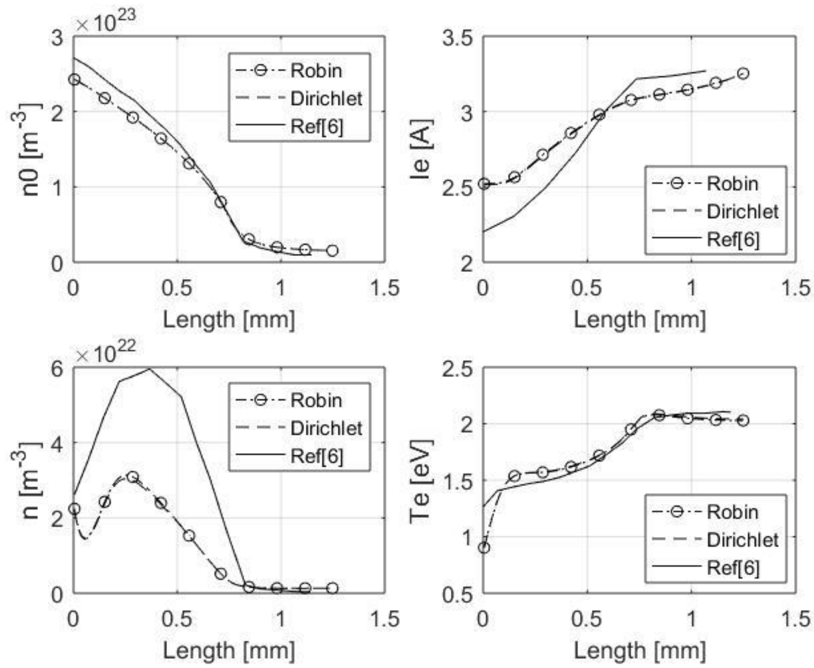

Figure III-1- BOL plasma profiles comparison: Dirichlet, Robin boundary conditions and numerical simulations from reference Ref. [6].

The small dip in the electron density located close to the inlet region, is not observed in other simulations of the NHC [6,9,14]; it might be due to an excessive low inlet electron temperature $T_e \sim 0.85$eV resulting from the insert 0D model, higher inlet T_e, about 1.7 eV, are indicated in [9,14] which might result from anomalous heating (resistivity) in the insert region.

This model does not include anomalous resistivity in the 0D insert region, however, if we force the inlet electron temperature to the value of 1.5, the value T_e settles immediately after the entrance region, we observe that the dip disappear and a dome shaped profile is recovered; this modification does not have a considerable impact on the plasma profiles solutions (see Figure III-2).

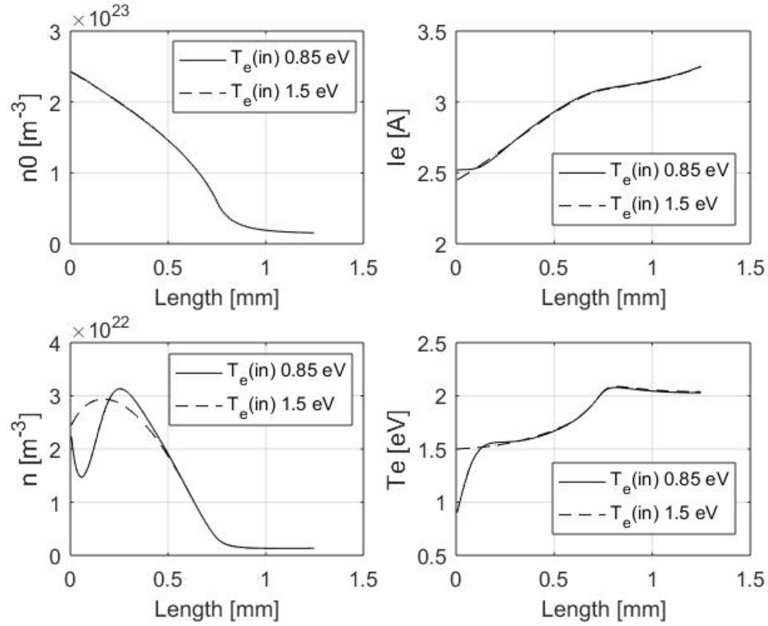

Figure III-2- Comparison of BOL profiles: inlet T_e calculated from insert and inlet T_e of 1.5 eV.

B. Orifice erosion profiles

The sputtering yield curve for tungsten material, as measured experimentally by Doerner [17] starts from 30 eV; since the energy of the ions inside the orifice channel is below such threshold, the yield curve is extended to cover the lower energy range. Mikellides proposes an Arrhenius form in Ref. [14], and then a further modified form [9] in order to match the measured erosion profile at 8200 h.
Figure III-3 show the comparison between the sputtering yield used in this work to match the erosion and the two curves before mentioned.

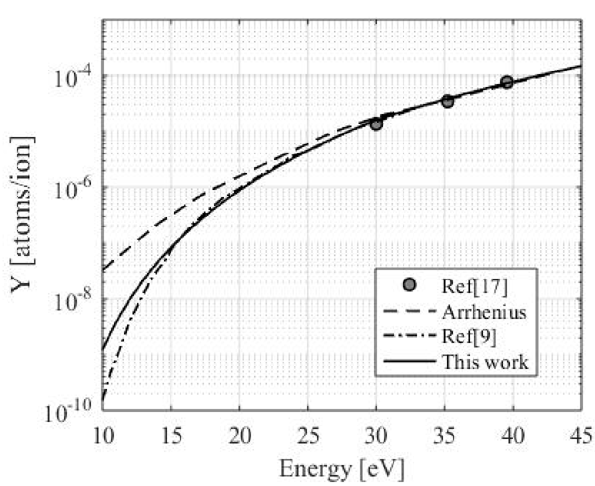

Figure III-3- Sputtering yields of W versus Xe ion energy, experimental data from Ref. [17] and numerical extrapolation from Ref. [9]

The change of the radius $R(x)$ due to sputtering fluxes is calculated as reported in Eq.22 , with M_w and ρ_w the mass and density of tungsten, and $\psi(\varphi)$ the sputtering yield calculated respect to the plasma potential.

$$\Delta R(x) = \frac{I_W}{e\,2\pi R} \cdot \Psi(\phi) \cdot \frac{M_W}{\rho_W}\,\Delta t \tag{22}$$

We constrained the forward time step so that the relative increment of the radius at each new simulation is $(R_{new} - R_{old})/R_{old} < 2 \cdot 10^{-3}$, this results in more than 400 simulations to reach the 8200 h target. Figure III-4 shows the temporal progression of the orifice internal surface at selected time steps, superimposed with the NHC experimental data at 8200 h. It is observed that the erosion rate decreases along the operation timeline, as the orifice channel progressively enlarges, both the plasma density and the plasma potential inside the orifice decreases; Figure III-5(left) shows this feature by plotting the maximum erosion rate along the channel and the maximum orifice radius along the straight section of the channel, versus the timeline.

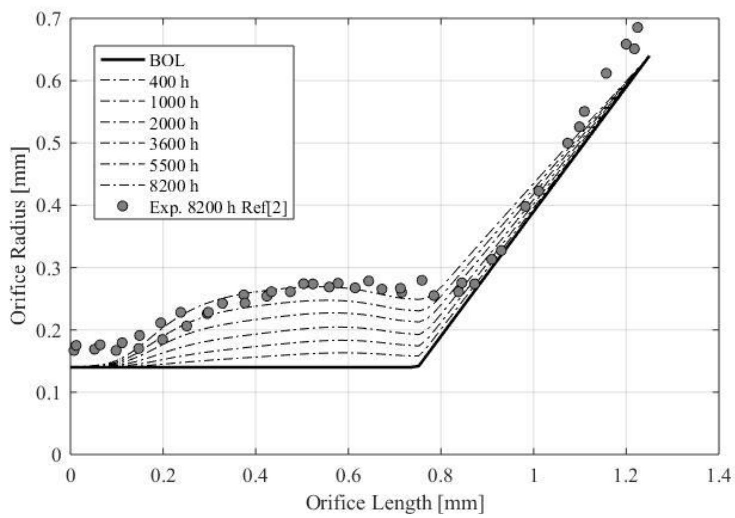

Figure III-4-Orifice radius profiles at different simulation time steps, experimental data from Ref. [2].

Figure III-5 (right) report the plasma potential along the orifice channel at BOL, for different values of the anomalous resistivity *'a'* coefficient in Eq.15 .

We have observed that one of the main effects of including the anomalous resistivity in the model, is to increase the electric field in the proximity of the throat region (straight to chamfered section at $x = 0.75\ mm$); this results in an increase of the plasma potential and it impacts considerably the erosion rate due to the exponential dependence of the sputtering yield on the ion energy.

The matching of the experimental data requires both tuning of the sputtering yield curve and the anomalous resistivity coefficient; the erosion simulation profiles in Figure III-4 were obtained setting $a = 0.08$, it was not possible to obtain an adequate match setting $a = 0$.

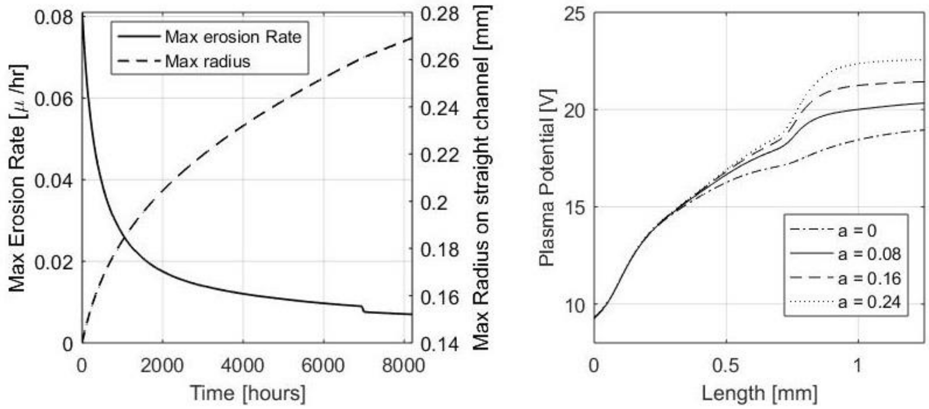

Figure III-5- (Left) max erosion rate and max channel radius in the straight section versus operation timeline; (right) plasma potential along the orifice channel for different values of the anomalous resistivity parameter.

IV. Conclusion

We present a one-dimensional model description of the HC orifice, to evaluate the temporal erosion resulting from sputtering of the channel wall; the model is coupled to a 0D (global-average) description of the insert region which provides boundary conditions for the 1D model.
The model is intended to be a low computing resource tool; in this test case, it runs more than 400 simulations to cover the 8200h of the NHC life-test [ref] with a total simulation time less than 10 hours.
It is shown that uncertainties related to the 0D description of the insert affects to a minor degree the 1D plasma profiles in the inlet region, and have negligible effect proceeding downstream the orifice channel. The 1D model calculates the plasma profiles and their evolution during the lifetime of the HC and it shows the expected reduction of erosion rate with the increase of the channel radius.
The experimental erosion profile is matched by adjusting the sputtering yield curve and anomalous resistivity *'a'* coefficient; the best match is found for $a = 0.08$, this value is found to be five times lower than the 0.4 value proposed in [9], while the sputtering yield curve is close to the curve proposed in [9]
The developed model is applicable to neutralizer hollow cathodes where the high pressure field makes the Poiseuille neutral flow assumption acceptable; in order to apply the model to discharge cathodes, a Navier-Stokes or a compressible-Euler solver needs to be implemented so that compressibility effects and sonic flow transitions are fully accounted.

References

1 Goebel, Dan M., and Ira Katz. Fundamentals of electric propulsion: ion and Hall thrusters. Vol. 1. John Wiley & Sons, 2008.

2 Polk, J., et al. "An overview of the results from an 8200 hour wear test of the NSTAR ion thruster." 35th Joint Propulsion Conference and Exhibit. 1999.

3 Capacci, Marco, et al. "Simple numerical model describing discharge parameters in orificed hollow cathode devices." 33rd Joint Propulsion Conference and Exhibit. 1997.

4 Katz, Ira, et al. "Sensitivity of hollow cathode performance to design and operating parameters." 35th Joint Propulsion Conference and Exhibit. 1999.

5 Wordingham, Christopher J., Pierre-Yves Taunay, and Edgar Choueiri. "A Critical Review of Orificed Hollow Cathode Modeling: 0D Models." 53rd AIAA/SAE/ASEE Joint Propulsion Conference. 2017.

6 Katz, Ira, et al. "One-dimensional hollow cathode model." Journal of Propulsion and Power 19.4 (2003): 595-600.

7 Albertoni, Riccardo, et al. "Numerical model for 100-kW class hollow cathodes part II." Proc. Space Propuls. 2010.

8 Coccaro, Fabio, et al. "Analytical approach for investigation of Hollow Cathode Orifice." Proc. Space Propuls. 2018.

9 Mikellides, Ioannis G., et al. "The discharge plasma in ion engine neutralizers: Numerical simulations and comparisons with laboratory data." Journal of Applied Physics 108.11 (2010): 113308.

10 Sary, Gaétan, Laurent Garrigues, and Jean-Pierre Boeuf. "Hollow cathode modeling: I. A coupled plasma thermal two-dimensional model." Plasma Sources Science and Technology 26.5 (2017): 055007.

11 Jameson, Kristina K., Dan M. Goebel, and Ron M. Watkins. "Hollow cathode and thruster discharge chamber plasma measurements." (2005).

12 Liu, Hui, et al. "2-D modelling of orificed hollow cathodes of stationary plasma thrusters SPT-100." IEEE Transactions on Plasma Science 43.12 (2015): 4024-4033.

13 Wordingham, Christopher J., Pierre-Yves Taunay, and Edgar Choueiri. "Theoretical Prediction of the Dense-Plasma Attachment Length in an Orificed Hollow Cathode." 35th IEPC International Electric Propulsion Conference, Atlanta, US. 2017.

14 Mikellides, Ioannis G., and Ira Katz. "Wear mechanisms in electron sources for ion propulsion, I: Neutralizer hollow cathode." Journal of Propulsion and Power 24.4 (2008): 855-865.

15 Mikellides, Ioannis G., et al. "Hollow cathode theory and experiment. II. A two-dimensional theoretical model of the emitter region." Journal of Applied Physics 98.11 (2005): 113303.

16 Moukalled, F., L. Mangani, and M. Darwish. "The finite volume method in computational fluid dynamics." An advanced introduction with OpenFoam® and Matlab®. Springer - 2016.

17 Doerner, R. P. "Low-energy sputtering yields of tungsten and tantalum." Journal of Vacuum Science & Technology A: Vacuum, Surfaces, and Films 23.6 (2005): 1545-1547.